Engineering Geology 114 (2010) 330–342

Contents lists available at ScienceDirect

Engineering Geology

journal homepage: www.elsevier.com/locate/enggeo

A geostatistical approach to mapping site response spectral amplifications

Eric M. Thompson [a,*], Laurie G. Baise [a], Robert E. Kayen [b], Yasuo Tanaka [c], Hajime Tanaka [a]

[a] 113 Anderson Hall, Tufts University, Medford, MA 02155, USA
[b] United States Geological Survey, Menlo Park, CA, USA
[c] Research Center for Urban Safety and Security, Kobe University, Japan

ARTICLE INFO

Article history:
Received 4 August 2009
Received in revised form 14 May 2010
Accepted 20 May 2010
Available online 1 June 2010

Keywords:
Seismic velocities
Site response
Geostatistics
Earthquake
Hazard
Map
Kobe
Microzonation

ABSTRACT

If quantitative estimates of the seismic properties do not exist at a location of interest then the site response spectral amplifications must be estimated from data collected at other locations. Currently, the most common approach employs correlations of site class with maps of surficial geology. Analogously, correlations of site class with topographic slope can be employed where the surficial geology is unknown. Our goal is to identify and validate a method to estimate site response with greater spatial resolution and accuracy for regions where additional effort is warranted. This method consists of three components: region-specific data collection, a spatial model for interpolating seismic properties, and a theoretical method for computing spectral amplifications from the interpolated seismic properties. We consider three spatial interpolation schemes: correlations with surficial geology, termed the geologic trend (GT), ordinary kriging (OK), and kriging with a trend (KT). We estimate the spectral amplifications from seismic properties using the square root of impedance method, thereby linking the frequency-dependent spectral amplifications to the depth-dependent seismic properties. Thus, the range of periods for which this method is applicable is limited by the depth of exploration. A dense survey of near-surface *S*-wave slowness (S_s) throughout Kobe, Japan shows that the geostatistical methods give more accurate estimates of S_s than the topographic slope and GT methods, and the OK and KT methods perform equally well. We prefer the KT model because it can be seamlessly integrated with geologic maps that cover larger regions. Empirical spectral amplifications show that the region-specific data achieve more accurate estimates of observed median short-period amplifications than the topographic slope method.

1. Introduction

The different factors that affect ground motions can be separated into three broad categories: source, path, and instrument (Lay and Wallace, 1995). Typically, the instrument response is known and can be deconvolved from recorded ground motions. Source effects include the location, dimensions and orientation of the fault, the slip distribution, and the rupture velocity. The path effects describe how the waveform is modified between the source and the instrument; this includes reflections, refractions, and phase conversions at subsurface structures, attenuation, and the generation of surface waves. The effect of the material within a few hundred meters of the surface is often termed site effects or site response.

It has long been recognized that near-surface geologic materials substantially modify recorded ground motions at frequencies that are important for seismic hazards analysis (e.g., Borcherdt, 1970; Shearer and Orcutt, 1987; Boore, 2004). The seismic properties of the near-surface materials that affect site response are the seismic slowness (*S*, inverse of velocity, *V*), density (ρ), and attenuation. Generally, the *S*-wave slowness (S_s), is considered the most important parameters to constrain.

The National Earthquake Hazard Reduction Program (NEHRP; ICC, 2006) site classifications are defined by $V_s(30)$, defined as 30 m divided by the *S*-wave travel time to 30 m depth. In situ measurements of V_s are both time consuming and expensive. This limits the number of locations where such data are available. Researchers have addressed this need primarily by developing spatial models to predict site class or spectral amplifications at unsampled locations (Tinsley and Fumal, 1985; Wills and Silva, 1998; Wills et al., 2000; Holzer et al., 2005; Wills and Clahan, 2006; Wald and Allen, 2007; Yong et al., 2008).

Three of these methods are similar in scale to this study. Tinsley and Fumal (1985) presented an index of site amplification for Los Angeles that is primarily based on soil type, age, and the average V_s of the unit. Holzer et al. (2005) developed a three-dimensional V_s model for a portion of the San Francisco Bay Area by combining stratigraphic and V_s information from 210 seismic cone penetration tests (SCPTs) and used the V_s model to map NEHRP site class. Yong et al. (2008) created maps that classify the range of $V_s(30)$ from satellite imagery for Islamabad, Pakistan.

* Corresponding author.
E-mail address: eric.thompson@tufts.edu (E.M. Thompson).

0013-7952/$ – see front matter © 2010 Elsevier B.V. All rights reserved.
doi:10.1016/j.enggeo.2010.05.010

Our goal is to identify and validate a method to estimate site response spectral amplifications with greater spatial resolution and accuracy than previous studies. Previous methods have focused on making predictions over large regions of interest, such as the state of California (Wills and Clahan, 2006) or the globe (Wald and Allen, 2007). The method we propose cannot be applied at such scales, and our goal is not to replace these methods. The methods outlined in this paper are appropriate for regions where special attention is warranted, such as urban regions exposed to moderate to high seismic risk. The method we employ consist of three components: (1) region-specific data collection, (2) a spatial model for interpolation of seismic properties, and (3) a theoretical method for computing spectral amplifications from the seismic properties.

Previously developed spatial models of site response can be organized in terms of increasing data availability and increasing model complexity. The Wald and Allen (2007) model does not require region-specific observations; this method correlates global topographic slope data (Farr and Kobrick, 2000) with NEHRP site class and utilizes previously published correlations of NEHRP site class with spectral amplifications (Borcherdt, 1994), herein termed the TS model.

Wills and Clahan (2006) developed a model for California that requires surficial geology maps, which are not available globally. Wills and Clahan (2006) compiled $V_s(30)$ measurements for sites throughout California and defined generalized surficial geologic units. Each unit is assigned a representative $V_s(30)$ value, which defines the NEHRP site class. The spectral amplifications can then be computed from the Borcherdt (1994) correlations.

We employ a separate but related method that we term the geologic trend (GT) method. An important aspect of this method is that seismic profiles are approximately evenly distributed throughout the region of interest. Note that this would be an inefficient strategy for a region the size of California. This is one reason why it is important to distinguish between the GT method and the Wills and Clahan (2006) method. Both methods, however, compute average V_s values for surficial geologic units. Limitations of the GT and Wills and Clahan (2006) approach include: (1) the mapped geology is a surface value while the $V_s(30)$ is a function of the materials at depths of 30 m, and (2) geologic maps are not typically collected with the application to correlations with V_s in mind (Tinsley and Fumal, 1985). Wills and Clahan (2006) compute only $V_s(30)$, but the GT method retains more of the available information in the soil profiles by computing the average S_s to a range of depths.

Aside from the GT model, we consider two alternative spatial interpolation techniques that expand on the geostatistical approach of Thompson et al. (2007). Specifically, we employ the geostatistical methods of ordinary kriging (OK) and kriging with a trend (KT). The geostatistical methods achieve a better spatial resolution than the GT model because they are capable of modeling variability within geologic units but also require more observations to achieve accurate results. We will address the accuracy of these models with a cross validation of the predicted S_s and comparisons of the predicted and observed spectral amplifications.

We also consider two alternative methods for linking seismic properties to spectral amplifications: the Borcherdt (1994) empirical correlations and the square root of impedance method (SRI), as described by Joyner et al. (1981). The Borcherdt (1994) correlations rely on a single site parameter for estimating the spectral amplifications, namely $V_s(30)$. In contrast, the SRI method links the depth-dependent seismic properties to the frequency-dependent site response amplification.

We choose to focus this study on the Kobe region because it is a densely populated urban area that is located in a deep sedimentary basin and exposed to heightened earthquake hazard. These characteristics are not unique to Kobe, but Kobe is distinguished from other such examples by the damage that was caused by the 1995 Hyogo-ken Nanbu earthquake. The maps of $V_s(30)$ presented in this article, along with the V_s profiles they are derived from, can be downloaded and viewed within the context of geographic, geotechnical, and earthquake effect data on the web-based geographic information system that we have created at http://gdcmaps.cee.tufts.edu/kobe/.

2. Data

We use the spectral analysis of surface waves (SASW) method (Nazarian and Stokoe, 1984; Stokoe et al., 1989) to estimate the S_s profiles following the methodology of Kayen et al. (2005). The SASW method has repeatedly fared well in blind comparisons to invasive measurements (Brown et al., 2002; Asten and Boore, 2005; Boore and Asten, 2008). Other surface wave methods, including passive source methods such as the multichannel analysis of surface waves (MASW) method (Park et al., 1999), may also provide inexpensive and efficient alternatives for mapping site response amplifications. Fig. 1(a) shows the locations of the 103 SASW sites included in our analysis. The geologic units are from the "Active Fault Map in Urban Area" map published by the Geographical Survey Institute of Japan at 1:25,000 scale.

The locations of the SASW surveys were chosen in two stages. First, the SASW sites were located at historical liquefaction sites for developing a deterministic and probabilistic model of liquefaction based on V_s (Kayen et al., 2010). Subsequently, the liquefaction data were augmented to extend the coverage to the edge of the basin. In the second stage, the goal was to keep the spacing between seismic profiles as uniform as possible while adding upper alluvial fan sites between the zone of liquefaction susceptible soil near the bay, and bedrock outcropping at the base of the Rokko Mountains. Specific locations were selected based on available space for seating the SASW seismometer array. Fig. 1(b) shows the locations of the temporary seismometer array that recorded aftershocks of the 1995 Hyogo-ken Nanbu earthquake (Iwata et al., 1996). We use these recordings to judge the accuracy of the different models in terms of spectral amplifications.

3. Methods

All calculations and analyses presented in this paper were completed with the free open-source software R (R Development Core Team, 2009) with the exception of the Wald and Allen (2007) topographic slope model discussed below, which was computed with Generic Mapping Tools (Wessel and Smith, 1991).

3.1. Topographic slope model

Wald and Allen (2007) presented a model that computes spectral amplifications from topographic slope. They compute slope from Shuttle Radar Topography Mission (SRTM) 30-sec global topography (Farr and Kobrick, 2000). This method predicts NEHRP site class based on empirical correlations of $V_s(30)$ with topographic slope. After obtaining site class from the topographic slope correlation, spectral amplifications can be estimated from the Borcherdt (1994) correlations with site class.

An important attribute of this model is that it is applicable across the entire globe, and thus it can be applied to Kobe. This also means that the resolution is relatively coarse: the 30-sec pixel size of the SRTM30 data is approximately a 1 km by 1 km square. We consider this model to be an appropriate baseline model to judge our proposed alternatives because it is the simplest available model, requiring minimal investment of time to obtain estimates of spectral amplifications. If we cannot improve on the Wald and Allen (2007) model, then the effort and investment into the dense SASW survey is not justified.

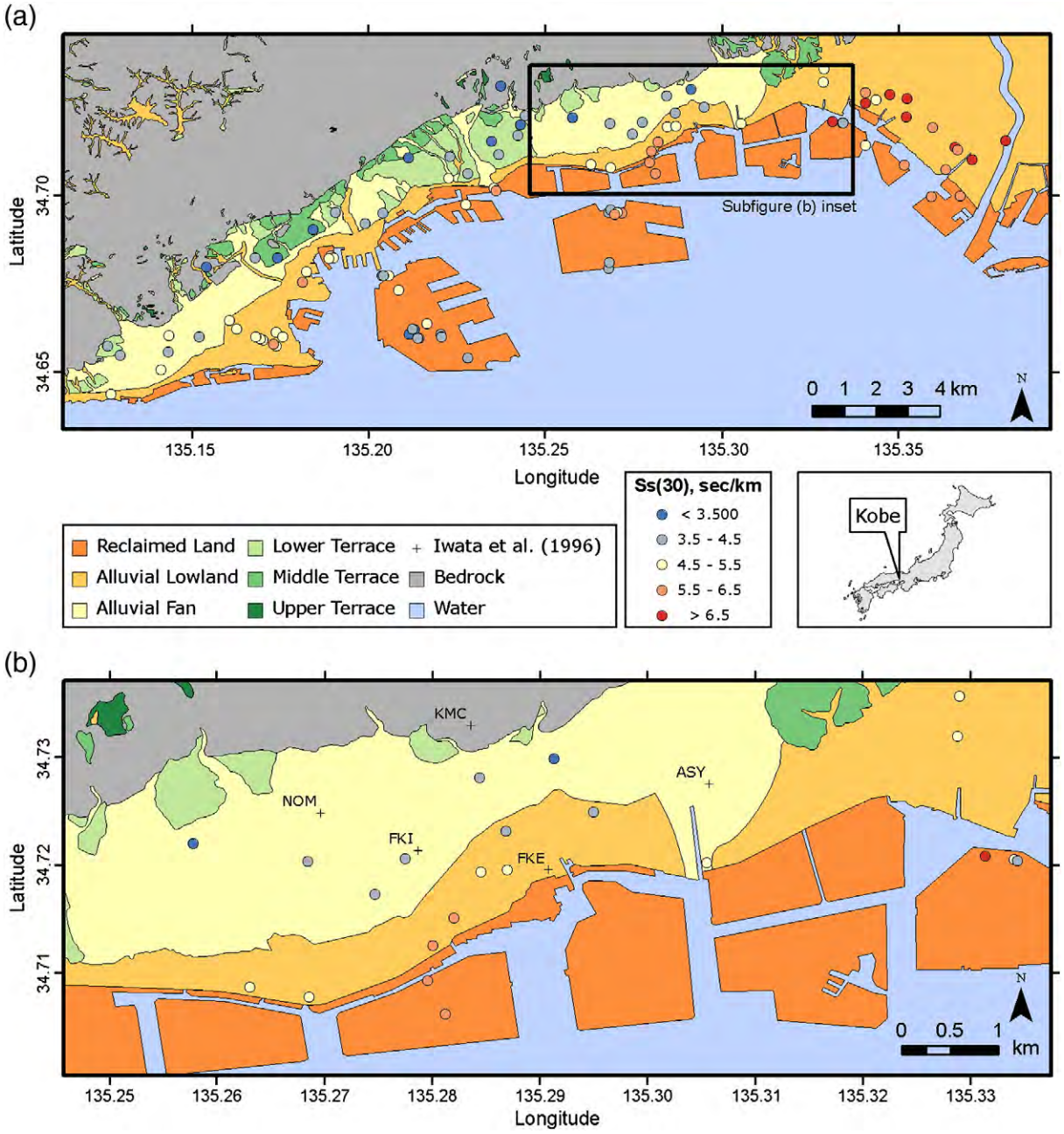

Fig. 1. (a) Geologic map of Kobe, Japan, and the site characterization locations. The $S_s(30)$ range is shown for each SASW site. (b) Locations where Iwata et al. (1996) recorded aftershocks of the Hyogo-Ken Nanbu earthquake.

3.2. Geologic trend model

The Wills and Silva (1998), Wills et al. (2000), and Wills and Clahan (2006) method for predicting $V_s(30)$ is based on previously mapped surficial geologic units. The underlying assumption of this method is that V_s, or at least $V_s(30)$, is approximately homogeneous within the spatial extent of surficial geologic units. Here, we must distinguish between the Wills and Clahan (2006) method and the specific model they develop. We use the term "Wills and Clahan (2006) method" to mean the process of correlating a seismic property with geologic units and predicting the expected value of that unit at all locations where that unit is mapped. In contrast, we use the term "Wills and Clahan (2006) model" to mean the specific correlations to the geologic units that they have derived. In this paper, we cannot apply the Wills and Clahan (2006) model because the geology of Kobe is different than the geology of California. Instead, we apply the Wills and Clahan (2006) method to Kobe, deriving new correlations of surficial geology with local SASW data. Additionally, we extend this method to a range of averaging depths, which can be paired with the SRI method for obtaining spectral amplifications (see Section 3.5). Throughout this paper, we refer to the spectral amplifications that result from pairing the SRI method with geologic correlations of S_s as the geologic trend (GT) model.

The primary variable of interest in this paper is

$$S_s(d) = \frac{1}{d}\int_0^d S_s dz \ , \tag{1}$$

which is computed for S_s as function of depth z. To express that $S_s(d)$ varies in space, we write $S_s(\mathbf{x}, d)$, where $\mathbf{x} = (x_1, x_2)$ is the two-

dimensional position vector. We assume that the distribution of $S_s(d)$ is lognormal. We are unaware of evidence that supports or contradicts this assumption. We choose the lognormal rather than the normal distribution simply because we require a non-negative distribution, although other distributional alternatives also meet this criteria.

Assuming a lognormal distribution, the mean of $\ln[S_s(\mathbf{x}, d)]$ is equal to the natural logarithm of the median of $S_s(\mathbf{x}, d)$:

$$\mu_{\ln(S)} = \ln\left[S_s^{\text{med}}(\mathbf{x}, d)\right], \tag{2}$$

where $S_s^{\text{med}}(\mathbf{x}, d)$ is the median of $S_s(\mathbf{x}, d)$. A maximum likelihood estimate for $S_s^{\text{med}}(\mathbf{x}, d)$ is

$$S_s^{\text{med}}(\mathbf{x}, d) = \exp\left(\frac{1}{n}\sum_{i=1}^{n}\ln[S_s(\mathbf{x}_i, d)]\right), \tag{3}$$

where $S_s(\mathbf{x}_i, d)$ are the n observed values of the random variable $S_s(\mathbf{x}, d)$for $i=1,2,\ldots,n$. A maximum likelihood estimate for the standard deviation is

$$S_{\ln}(\mathbf{x}, d) = \sqrt{\frac{1}{n}\sum_{i=1}^{n}\left(\ln[S_s(\mathbf{x}_i, d)] - S_s^{\text{med}}(\mathbf{x}, d)\right)^2}. \tag{4}$$

3.3. Geostatistical models

We use the geostatistical method of kriging to estimate $S_s(\mathbf{x}, d)$ at unsampled locations from the observed values. Kriging is a generalized least-squares regression algorithm. Following a formulation from Cressie (1993), we model $S_s(\mathbf{x}, d)$ as a random field that varies in space as

$$S_s(\mathbf{x}, d) \equiv \mu(\mathbf{x}, d) + \delta(\mathbf{x}, d), \tag{5}$$

where the deterministic model $\mu(\mathbf{x}, d)$ describes the spatial fluctuation of the mean, and the correlated error process $\delta(\mathbf{x}, d)$ includes any spatially-uncorrelated measurement error (white noise) and the spatially-correlated zero-mean fluctuation of $S_s(\mathbf{x}, d)$ about $\mu(\mathbf{x}, d)$.

The kriging linear regression estimator of $S_s(\mathbf{x}, d)$ is defined as

$$S_s^*(\mathbf{x}, d) = \sum_{i=1}^{n}\lambda_i[S_s(\mathbf{x}_i, d) - \mu(\mathbf{x}_i, d)] + \mu(\mathbf{x}, d), \tag{6}$$

where λ_i are weights assigned to the different observations computed by minimizing the error variance $\sigma_E^2(\mathbf{x}, d) = \text{Var}[S_s^*(\mathbf{x}, d) - S_s(\mathbf{x}, d)]$.

The different types of kriging are defined by how $\mu(\mathbf{x}, d)$ is modeled. Simple kriging (SK) assumes that $\mu(\mathbf{x}, d)$ is known and constant, ordinary kriging (OK) assumes $\mu(\mathbf{x}, d)$ is unknown but still constant, and kriging with a trend (KT), also known as "universal kriging," allows $\mu(\mathbf{x}, d)$ to fluctuate in space (Goovaerts, 1999).

If $\mu(\mathbf{x}, d)$ is a function of external or secondary data (i.e., not defined as a function of $S_s(\mathbf{x}_i, d)$), then the KT method can be implemented in three steps: (1) detrend the data by subtracting $\mu(\mathbf{x}, d)$ from the $S_s(\mathbf{x}_i, d)$ to get $\delta(\mathbf{x}_i, d)$, (2) estimate $\delta(\mathbf{x}, d)$ throughout the region of interest with SK, and (3) add back $\mu(\mathbf{x}, d)$ to $\delta(\mathbf{x}, d)$ to get $S_s^*(\mathbf{x}, d)$ (Goovaerts, 1999). For the KT model, we define $\mu(\mathbf{x}, d)$ as $S_s^{\text{med}}(\mathbf{x}, d)$ (i.e., the GT model).

To characterize the spatial correlation structure of $S_s(\mathbf{x}, d)$, it is convenient to plot the variance as a function of separation distance

$$2\gamma(\mathbf{h}) = Var[S_s(\mathbf{x}_1, d) - S_s(\mathbf{x}_2, d)] \tag{7}$$

where $\mathbf{h}$ is the Euclidean distance between two locations $\mathbf{x}_1$ and $\mathbf{x}_2$, and $2\gamma(\mathbf{h})$ is termed the variogram. It is common to describe the spatial correlation structure with the semivariogram, $\gamma(\mathbf{h})$, rather than the variogram. The semivariogram can be estimated from data with

$$\hat{\gamma}(\mathbf{h}) = \frac{1}{2N(\mathbf{h})}\sum_{N(\mathbf{h})}\left[S_s(\mathbf{x}_i, d) - S_s\left(\mathbf{x}_j, d\right)\right]^2, \tag{8}$$

where the sum is over all i and j (i.e., all pairs of observations), and $N(\mathbf{h})$ is the number of measurements for a given class of $\mathbf{h}$.

Once the measurements have been demonstrated to exhibit a strong spatial dependence by noting an increase in the experimental semivariogram $\hat{\gamma}(\mathbf{h})$ as $\mathbf{h}$ increases, we need to model the spatial structure with a conditionally negative definite function to compute the weights λ_i in Eq. (6). Typically, $\hat{\gamma}(\mathbf{h})$ will remain constant for $\mathbf{h}>\phi$; ϕ and $\hat{\gamma}(\mathbf{h}=\phi)$ are termed the range and sill, respectively.

One may expect that $\hat{\gamma}(\mathbf{h})$ should approach zero at $\mathbf{h}=0$, which indicates that points in the same location have the same value. However, this rarely occurs in real data. The value of $\hat{\gamma}(\mathbf{h})$ at $\mathbf{h}=0$ is called the nugget, and can be interpreted as the measurement error or the amount of variability within the sample.

The semivariogram model we choose is a generalization of the exponential model, termed the Whittle–Matérn model

$$\gamma(\mathbf{h}) = \sigma^2\left[1 - \frac{2^{1-\nu}}{\Gamma(\nu)}\left(\frac{\mathbf{h}}{a}\right)^{\nu}K_{\nu}\left(\frac{\mathbf{h}}{a}\right)\right] + \tau, \tag{9}$$

where σ^2 is the partial sill, τ is the nugget, a is the range parameter, ν is the shape parameter, K_{ν} is the modified Bessel function of the second kind of order ν, and $\Gamma(\cdot)$ is the gamma function (Diggle and Ribeiro, 2006; Morgan et al., 2008). Note that the complete sill variance is $\sigma^2+\tau$. Guttorp and Gneiting (2005) discuss the different names that are given to this model depending on the field of study.

3.4. Spectral amplifications from empirical correlations

Borcherdt (1994) developed a simple methodology for estimating the spectral amplifications as a function of input ground motion intensity and NEHRP site class or $V_s(30)$. The equations that Borcherdt (1994) presented are empirical correlations developed from recorded ground motions primarily from the San Francisco and Los Angeles regions with additional data from Salt Lake City, Seattle, and Memphis. Including the ground motion intensity as an input parameter gives the equations the flexibility to model the nonlinear damping behavior of soils. Borcherdt (1994) defined the short-period

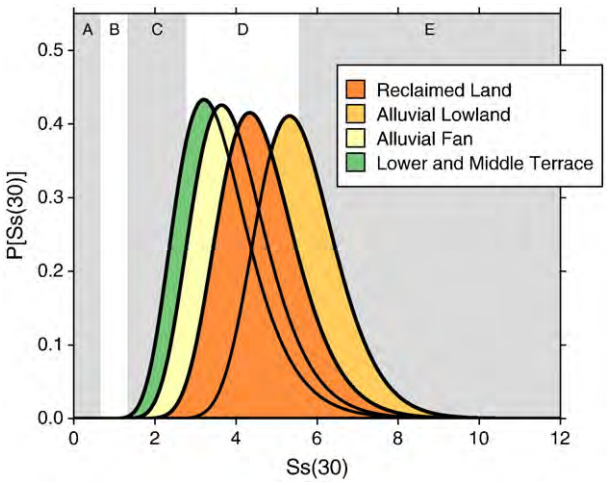

Fig. 2. Density functions for $S_s(30)$ by geologic unit in Kobe, Japan. We assume that the density functions are lognormal. Shaded polygons indicate the range of NEHRP site classes A through E.

(0.1–0.5 s) and mid-period (0.4–2 s) amplification factors, F_a and F_v, as

$$F_a = [V_s^{\mathrm{ref}}(30)/V_s(30)]^{m_a} \quad , \tag{10}$$

$$F_v = [V_s^{\mathrm{ref}}(30)/V_s(30)]^{m_v} \quad , \tag{11}$$

where $V_s^{\mathrm{ref}}(30)$ is the $V_s(30)$ of the reference site, and m_a and m_v are constants that are selected as a function of input ground motion intensity from Table 2 of Borcherdt (1994). In this paper, however, we restrict our analysis to ground motions in the linear range. Thus, for all cases in this paper, $m_a = 0.35$ and $m_v = 0.65$. If a quantitative estimate of $V_s(30)$ is unavailable but the site class can be inferred, then the amplification factors can also be selected from Table 2 of Borcherdt (1994).

3.5. Square root of impedance model

The plane *SH*-wave (the horizontally polarized component of the *S* wave) amplifications can be computed exactly for all reflections and refractions within a horizontally stratified medium over a non-attenuating halfspace, termed the SH1D model (Thomson, 1950; Haskell, 1953). A shortcoming of this method is that the peaks and valleys of amplifications are sensitive to details of the seismic profile that are not known with confidence (Brown et al., 2002). Additionally, Joyner et al. (1981) showed that the dominant process that

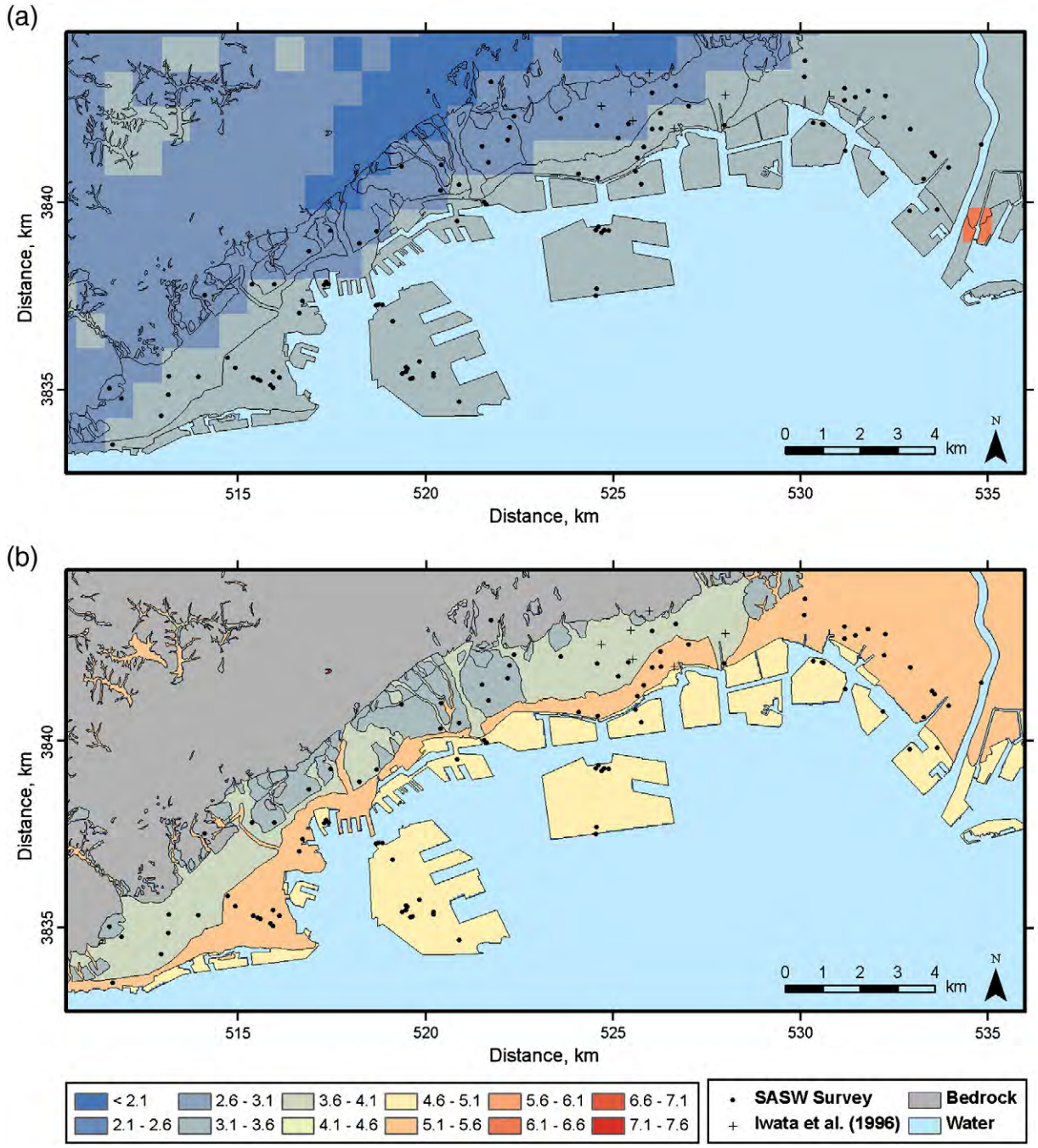

Fig. 3. Maps of S_S^p (**x**, 30) for (a) the Wald and Allen (2007) topographic slope method (TS), and (b) the geologic trend (GT) method, which is based on the local SASW measurements.

contributes to site amplification is the passing of seismic waves from a higher impedance material into a lower impedance material, where impedance is defined as $\rho \times V$, and the resonance that is created by the interference of multiply reflected waves is less important. The resonance effect of reflected waves is likely to be diminished because of the natural heterogeneity that is inherent in natural materials, which cannot be accounted for in one-dimensional models (Thompson et al., 2009). The SRI method is also based on averaged material properties, which exhibit stronger spatial dependence than more detailed properties, making the averaged values more appropriate for geostatistical interpolation (Baise et al., 2008).

The SRI method derives its name from the relationship between the amplitude (A) of a seismic wave to the impedance of the medium. Shearer (1999) shows that if the impedance varies in space, then the amplitude varies as

$$\frac{A_2}{A_1} = \sqrt{\frac{\rho_1 V_1}{\rho_2 V_2}}\ , \tag{12}$$

assuming that the energy in the seismic wave is completely transmitted from one material to the other. If Eq. (12) is put in terms of S rather than V, then we see that the amplification is directly proportional to $\sqrt{S_2 / S_1}$. This is why the primary variable of interest in this paper is $S_s(d)$ (Eq. (1)) rather than $V_s(d)$ (see also Brown et al., 2002).

Restricting our analysis to the averaged value of V_s to a single depth, typically 30 m, is undesirable because the resulting approximation does not account for the depth dependence of the seismic properties which influence the frequency dependence of the spectral amplifications. We generalize $V_s(30)$ to $V_s(d)$, and use its inverse $S_s(d)$. These values are related to the frequency (f) dependence of amplification, $A(f)$, through the quarter wavelength approximation

$$f(d) = \frac{1}{4\, d\, S_s^p(d)}\ , \tag{13}$$

$$A[f(d)] = \exp(-\pi\kappa_0 f)\sqrt{\frac{\rho^r S_s^p(d)}{\rho^s S_s^r}}\ , \tag{14}$$

where S_s^r and ρ^r are the S-wave slowness and density of the material at the hypocenter of the source, ρ^s is the density of the surficial material, κ_0 is the attenuation parameter, and $S_s^p(d)$ is the predicted value of $S_s(d)$. Note that $S_s^p(\mathbf{x}, d)$ corresponds to $S_s^{\mathrm{med}}(\mathbf{x}, \mathrm{d})$for the GT model (Eq. (3) and to $S_s^*(\mathbf{x}, \mathrm{d})$ for the OK and KT models (Eq. (6)).

A map of $A(f)$ for a given f (or range of f) is more useful for seismic hazard analysis than a map of $V_s(30)$. To achieve this, we compute $S_s^p(d)$ for $d = 1, 2, \ldots, 30$ m at the location of interest and for each of the GT, OK, or KT methods. Then for each d, we compute f and $A(f)$ from Eqs. (13) and (14) and linearly interpolate the $A(f)$ to the frequency of interest. The map is produced by repeating this procedure for every point on a regularly spaced grid that spans the area of interest. We use a grid spacing of 51 m for all maps of $S_s^p(d)$.

We assume $S_s^r = 0.289$ s/km and $\rho^r = 2.7$ for the rock in the vicinity of the hypocenter. These values are taken from Table 2 of Pitarka et al. (1998), which reports the bedrock parameters that they chose for the three-dimensional model of the Kobe region. We also assume $\rho^s = 2.0$. Following Boore and Joyner (1997), we assume $\kappa_0 = 0.035$. Note that we also must divide $A(f)$ by the $A(f)$ for the reference site. For this, we assume the S_s and ρ profiles published by Iwata et al. (1996) for site KMC (see Fig. 1(b) and the discussion of reference sites in Section 3.7).

3.6. Cross validation

We employ the "leave-one-out" cross validation method for each of the spatial models derived from the local SASW data (see Harrell, 2006, for a discussion of different validation methods). Considering each spatial model independently, and for each of $n = 103$ samples, the spatial model is built as though that sample did not exist. Then the value at the location of the removed sample is estimated with the new model. Thus, for each spatial model we have a complete set of n $S_s^p(\mathbf{x}, \mathrm{d})$ which we compare to $S_s(\mathbf{x}_i, d)$ to quantify model performance.

This procedure can be thought of as a k-fold cross validation where $k = n$. For the two kriging models, we estimate the empirical semivariogram and optimize the model parameters after removal of each observation. Then we compute $S_s^p(\mathbf{x}, d)$ from Eq. (6) at the location of the removed observation. For the GT model, $S_s^p(\mathbf{x}, d)$ is computed from Eq. (3) for all observations within the same geologic classification as the removed sample.

Legates and McCabe (1999) compare different methods for evaluating the goodness-of-fit of a model. They conclude that correlation-based methods, such as the coefficient of determination (R^2), are insensitive to additive and proportional differences between predictions and observations. They advocate for the coefficient of efficiency

$$E = 1 - \frac{\sum_{i=1}^{n}\left[S_s(\mathbf{x}_i, d) - S_s^p(\mathbf{x}, \mathrm{d})\right]^2}{\sum_{i=1}^{n}\left[S_s(\mathbf{x}_i, d) - \bar{S}_s(\mathbf{x}, \mathrm{d})\right]^2}, \tag{15}$$

where $\bar{S}_s(\mathbf{x}, d)$ is the sample mean of $S_s(\mathbf{x}_i, d)$, and the possible values of E include the interval $(-\infty, 1)$. E is sensitive to additive and proportional differences, and E is easier to interpret in terms of model performance than are correlation-based parameters (Legates and McCabe, 1999). The numerator in Eq. (15) is the mean square error of the model, while the denominator is the variance of the observed data. It is easy to see that if $S_s^p(\mathbf{x}, d) = \bar{S}_s(\mathrm{x}, d)$ (i.e., the model simply predicts the mean value of the observations everywhere) then $E = 0$. Thus, any model where $E \le 0$ should be rejected because a model that simply predicts the mean of the observations would perform better. If $E = 1$, then predicted values exactly match the observed values.

3.7. Response spectra

Pseudospectral acceleration (PSA) is a convenient parameter for describing a ground motion. This representation is particularly

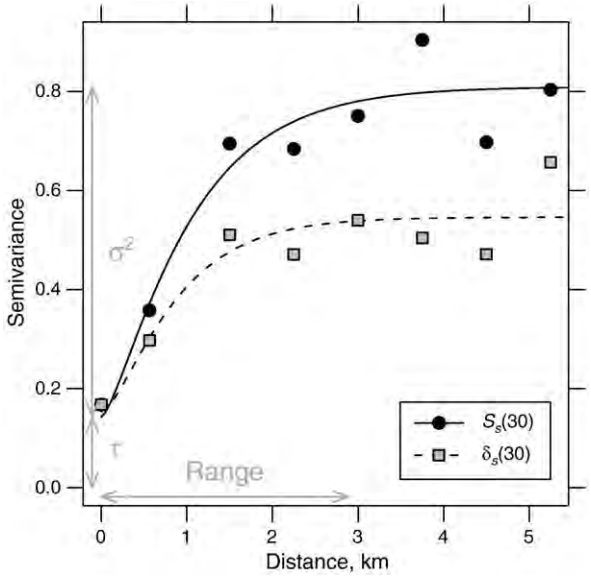

Fig. 4. Empirical (symbols) and model (curve) semivariograms for $S_s(\mathbf{x},30)$ (for the OK model) and $\delta(\mathbf{x},30)$ (for the KT model). For illustration, we have labeled τ, σ^2, and the range on the $S_s(\mathbf{x},30)$ model semivariogram.

meaningful from an engineering perspective because the PSA at period T is the maximum acceleration of a single-degree-of-freedom (SDOF) system with damping ratio ξ and natural period T in response to the input ground motion (Kramer, 1996). We compute an orientation-independent PSA(T) termed GMRotI50 by Boore et al. (2006). We employ the Boore (2008) Fortran programs to compute GMRotI50. GMRotI50 is derived from the set of geometric means of the two horizontal components rotated to all possible orthogonal rotation angles (see Boore et al., 2006, for further details). Following convention, all PSA(T) in this article are for a SDOF system with $\xi = 5\%$.

This article is concerned with site response, but many other factors influence the recorded ground motions at a site. Assuming that the observed seismogram is exactly the combination of linear time-invariant systems (source, path, and instrument), we can isolate the site response by dividing the PSA(T) of the recording that includes site response by the PSA(T) of the recording that contains no site effects

$$a(T) = \frac{\mathrm{PSA}(T)}{\mathrm{PSA}^{\mathrm{ref}}(T)} \quad , \tag{16}$$

where $\mathrm{PSA}^{\mathrm{ref}}(T)$ is the PSA(T) at the reference site. Note that $A(T)$ refers to the amplifications predicted by the assumptions of the SRI method (Eq. (14)), while $a(T)$ is an empirical estimate of site response from pairs of recorded ground motions. Two types of ground motion pairs are typically employed to isolate site response. If both receivers are located at the free surface and the reference site is seated on

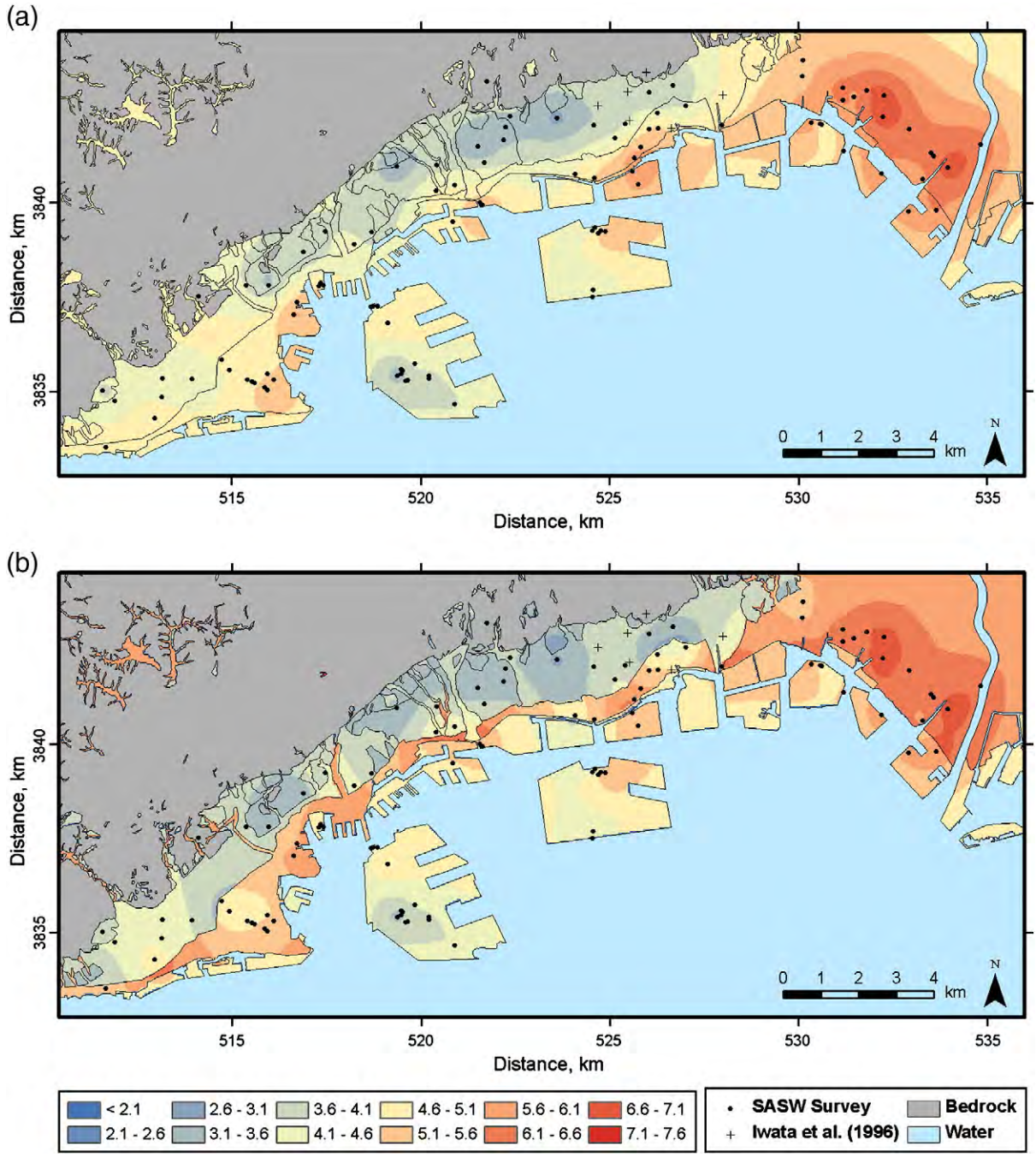

Fig. 5. Maps of $S_S^p(\mathbf{x},30)$ for (a) ordinary kriging (OK), and (b) kriging with a trend (KT).

outcropping bedrock then the receivers are categorized as a soil-outcrop pair. Alternatively, if one receiver is located at the free surface and the other is located beneath it then the receivers are categorized as a surface-downhole pair.

A soil-outcrop pair is more conceptually intuitive because the resulting $a(T)$ represents the transfer function that is often desired in practical applications, such as modifying a synthetic ground motion or a previously recorded rock motion to include the site response. All site response transfer functions in this paper are computed for a soil-outcrop pair where the outcrop motion is derived from site KMC in Fig. 1 (b).

The assumption that the reference site is free of site effects can be severely violated for most soil-outcrop pairs, biasing the transfer function. Detailed studies of surface-downhole receiver arrays by Abercrombie (1997) demonstrated that even very hard outcropping rock modifies the wavefield as it approaches the surface.

We assume that $a(T)$ follows a lognormal distribution. Thus, we simply modify Eq. (3) to compute the median of $a(T)$, termed $a^{\text{med}}(T)$.

4. Results

4.1. Topographic slope and geologic trend models

Fig. 2 shows the lognormal density functions for $S_s(30)$ within most of the geologic units illustrated in Fig. 1. The density functions in Fig. 2 show that the differences in the median of the Kobe $S_s(\mathbf{x},30)$ are small. In general, we expect the GT model to perform better when the distributions of the geologic units exhibit more separability. The relatively large amount of overlap of the distributions could be attributed to the fact that our samples in Kobe are all from young sedimentary units.

Fig. 3 presents maps of $S_s^p(\mathbf{x},30)$ for (a) the TS model and (b) GT model. These figures show that the GT map is more detailed than the more widely applicable TS map. Both maps show a similar trend of increasing $S_s^p(\mathbf{x},30)$ toward the coast; however, the TS map exhibits significantly smaller values of $S_s^p(\mathbf{x},30)$ than the GT map.

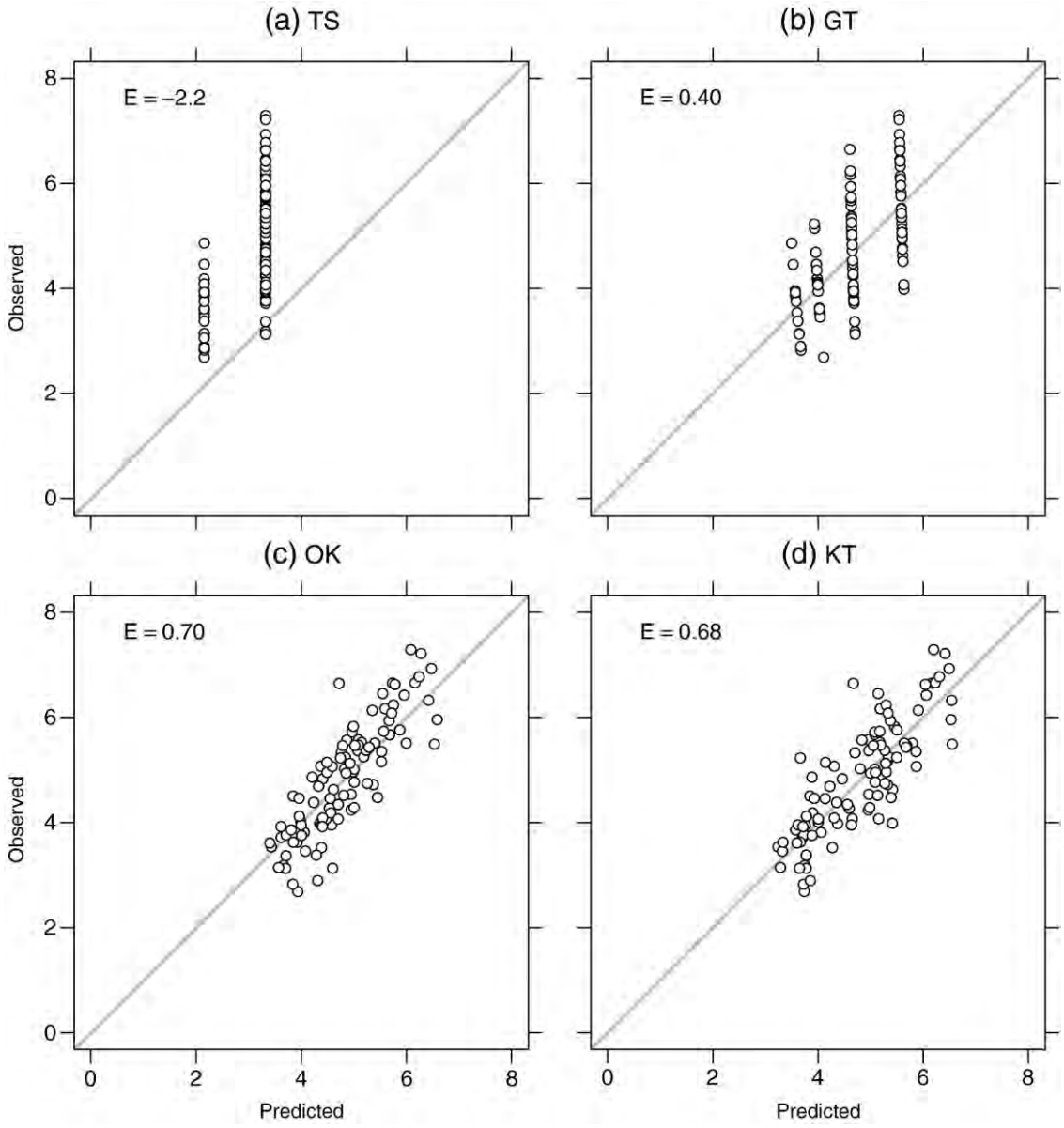

Fig. 6. Cross validation of four methods for computing $S_s^p(\mathbf{x},30)$.

4.2. Geostatistical models

The ability of kriging to model a spatially variable property such as S_s must first be judged by inspection of the empirical semivariogram. If the data are not characterized by a strong spatial correlation structure, then kriging cannot accurately model the data. Fig. 4 shows the empirical and model semivariograms of $S_s(\mathbf{x},30)$ and $\delta_s(\mathbf{x}, d)$. Note that the semivariogram of $S_s(\mathbf{x},30)$ is pertinent to the OK model, and the semivariogram of $\delta_s(\mathbf{x}, d)$ is pertinent to the KT model. For illustration, we have labeled τ, σ^2, and the range on the $S_s(\mathbf{x},30)$ model semivariogram.

Fig. 4 shows that the sill variance $(\sigma^2+\tau)$ of $\delta(\mathbf{x},30)$is about 33% smaller than that of $S_s(\mathbf{x},30)$. This indicates that $\mu(\mathbf{x}, d)$ is accounting for a significant portion of the variability in the KT model.

The nugget-to-sill ratio approximates the strength of the spatial dependence of the data (Cambardella et al., 1994). Cambardella et al. (1994) proposed that a ratio smaller than 0.25 indicates strong spatial dependence, a ratio of 0.25 to 0.75 indicates moderate spatial dependence, and a ratio greater than 0.75 indicates weak spatial dependence. The nugget-to-sill ratio is 0.22, 0.20, and 0.21 for $S_s(\mathbf{x},10)$, $S_s(\mathbf{x},20)$, and $S_s(\mathbf{x},30)$, respectively. The nugget-to-sill ratio is 0.27, 0.25, and 0.39 for $\delta(\mathbf{x},10)$, $\delta(\mathbf{x},20)$, and $\delta(\mathbf{x},30)$, respectively. Thus, both OK and KT should perform well in this region for a spectrum of averaging depths.

Fig. 5 presents maps of $S_s^p(\mathbf{x},30)$ using the two geostatistical methods (OK and KT). As seen in Fig. 5(a), the OK method ignores geologic boundaries. The inclusion of geologic units into the KT model is seen in Fig. 5(b) as discontinuities of $S_s^p(\mathbf{x},30)$ at the geologic unit

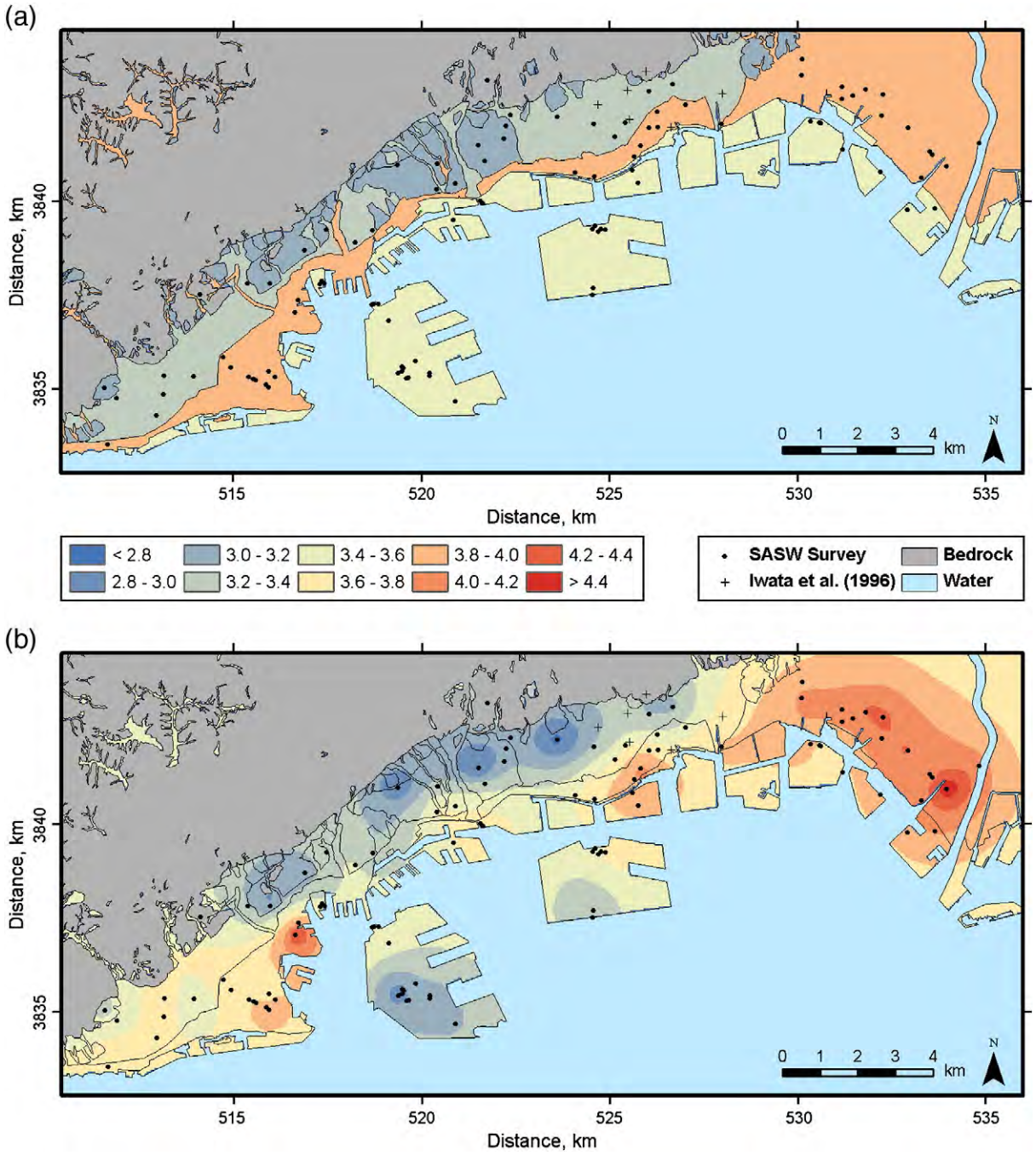

Fig. 7. Maps of 3 Hz spectral amplifications for (a) the geologic trend (GT) model, (b) the ordinary kriging (OK) model, and (c) the kriging with a trend (KT) model.

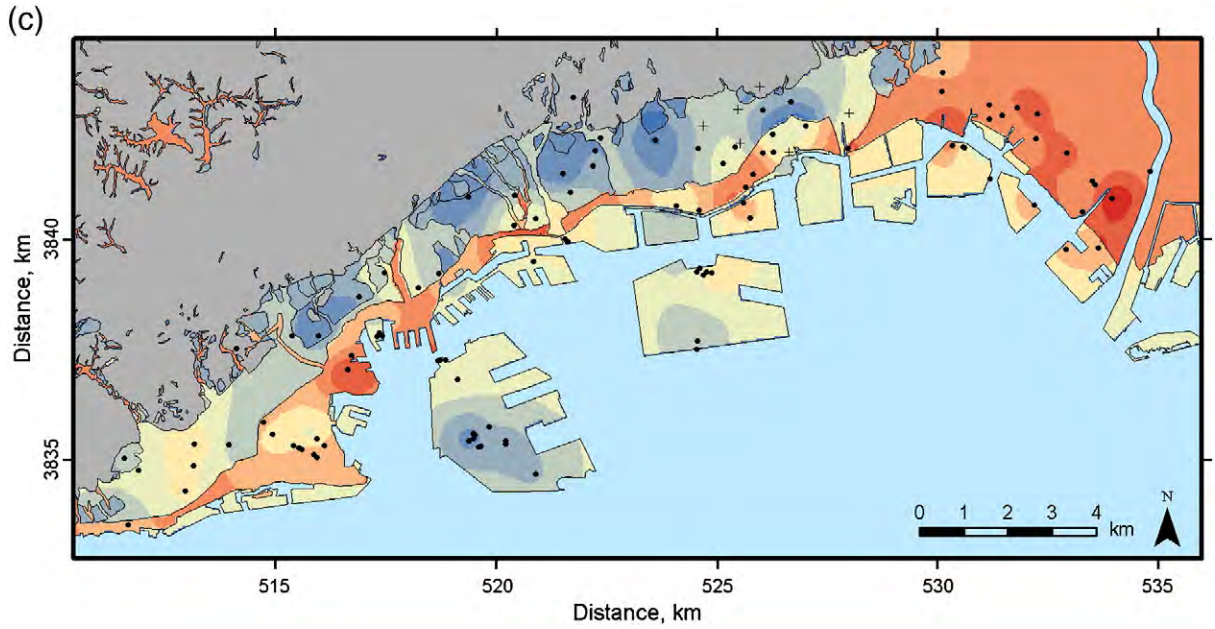

Fig. 7 (*continued*).

interfaces. Note that the three maps representing the GT, OK, and KT models use local SASW measurements and show similar trends. Only the geostatistical methods, however, allow for spatial variability within a geologic unit.

4.3. Cross validation

Fig. 6 summarizes the cross validation of the four spatial models. The TS and GT $S_s^p(\mathbf{x},30)$ are binned because of the discrete nature of the predictions. The three methods that use the local SASW data are validated with the "leave-one-out" procedure. But cross validation is not applicable to the TS method because it was not developed with the SASW data. The TS $S_s^p(\mathbf{x},30)$ are simply compared to $S_s(\mathbf{x}_i,30)$. Note that $E>0$ for the three models that use the local SASW data, but $E<0$ for the TS model.

Both OK and KT outperform GT, but the difference in performance between OK and KT is negligible. Thus, Fig. 6 and the associated values of E provide no insight into which geostatistical method will perform better.

4.4. Spectral amplification maps

The maps of $S_s^p(\mathbf{x},30)$ in Figs. 3 and 5 can easily be paired with the Borcherdt (1994) equations for estimating spectral amplifications. The maps of $A(f=3\text{ Hz})$ in Fig. 7, however, are derived from the SRI method, where $S_s^p(\mathbf{x}, d)$ is computed from (a) the GT model, (b) the OK model, and (c) the KT model. We use $f=3$ Hz because it is approximately the midpoint of the Borcherdt (1994) short-period passband (0.1–0.5 s). The minimum usable f is determined by both the maximum d and the value of $S_s(d)$ as indicated by Eq. (13). Thus, $A(f)$ for longer periods require deeper profiles. Although we see that there are locations where the three models predict different amplifications, we cannot yet determine which model performs better than the others.

4.5. Ground motion validation

If our final goal is to compute $A(f)$ from the SASW data, then the most appropriate form of validation is to compare $A(f)$ to $a(T)$. Iwata et al. (1996) recorded aftershocks (for which $2.9\leq M_{JMA}\leq 4.9$) of the 1995 Hyogo-ken Nanbu earthquake at five soil sites and a reference rock site. The ground motion data are not available for one of the soil sites, which leaves four soil sites (NOM, FKI, FKE, and ASY) with which we compute PSA(T) as described in Section 3.7. The locations of these sites and the reference rock site (KMC) are shown in Fig. 1 (b).

Fig. 8 compares the $a(T)$ to the $A(f)$ computed from the TS, GT, OK, and KT models. Additionally, Fig. 8 includes the amplifications that result when Eqs. (10) and (11) (Borcherdt, 1994) are combined with the GT model, denoted GT + B (discussed in more detail below). Although the inter-event scatter is large, Fig. 8 shows that the $a^{med}(T)$ at sites FKI, FKE, and ASY is more accurately modeled by the $A(f)$ computed from the GT, OK, and KT models than the TS and GT + B models. The $a^{med}(T)$ at NOM, in contrast, exhibit a distinct peak between 0.1 and 0.2 s that is not reflected in any of the models. It is also important to note that the GT, OK, and KT models result in nearly identical $A(f)$, especially when compared to the amount of inter-event variability of $a(T)$. These models, however, are closer to the $a^{med}(T)$ than the amplifications predicted by the TS or GT + B models, even for site NOM.

There are two factors that contribute to the relatively poor performance of the TS method in Fig. 8: (1) The $S_s^p(\mathbf{x},30)$ values are underpredicted in Kobe by the correlation with topographic slope, as illustrated by Fig. 6; and (2) Eqs. (10) and (11) are a relatively coarse approximation of spectral amplifications. We separate the effect of the Borcherdt (1994) approximation by applying Eqs. (10) and (11) to $S_s^{med}(\mathbf{x}, 30)$, termed the GT + B model. We assume $V_s^{ref}(30)=1200$ m/sec (from the Iwata et al. (1996) V_s profile for KMC). The GT + B model still underpredicts the short-period amplifications, but substantially improves the predictions compared to the TS model. Additionally, the GT + B model performs relatively well for the mid-period passband (0.4–2 sec), which cannot be computed from the SASW data due to the limited depth of exploration in this dataset. Thus, a substantial percentage of the TS model misfit in Fig. 8 stems from the approximation of the Borcherdt (1994) equations.

We may expect the spatial models to perform poorly at NOM if S_s exhibits a distinct spatial trend that is not captured by the spatial models because of the limited spatial extent of the S_s data. If this is the source of the bias then the bias could be reduced by collecting more data. We think this is an unlikely explanation for the misfit at NOM because it is actually located closer to SASW profiles than site ASY, and

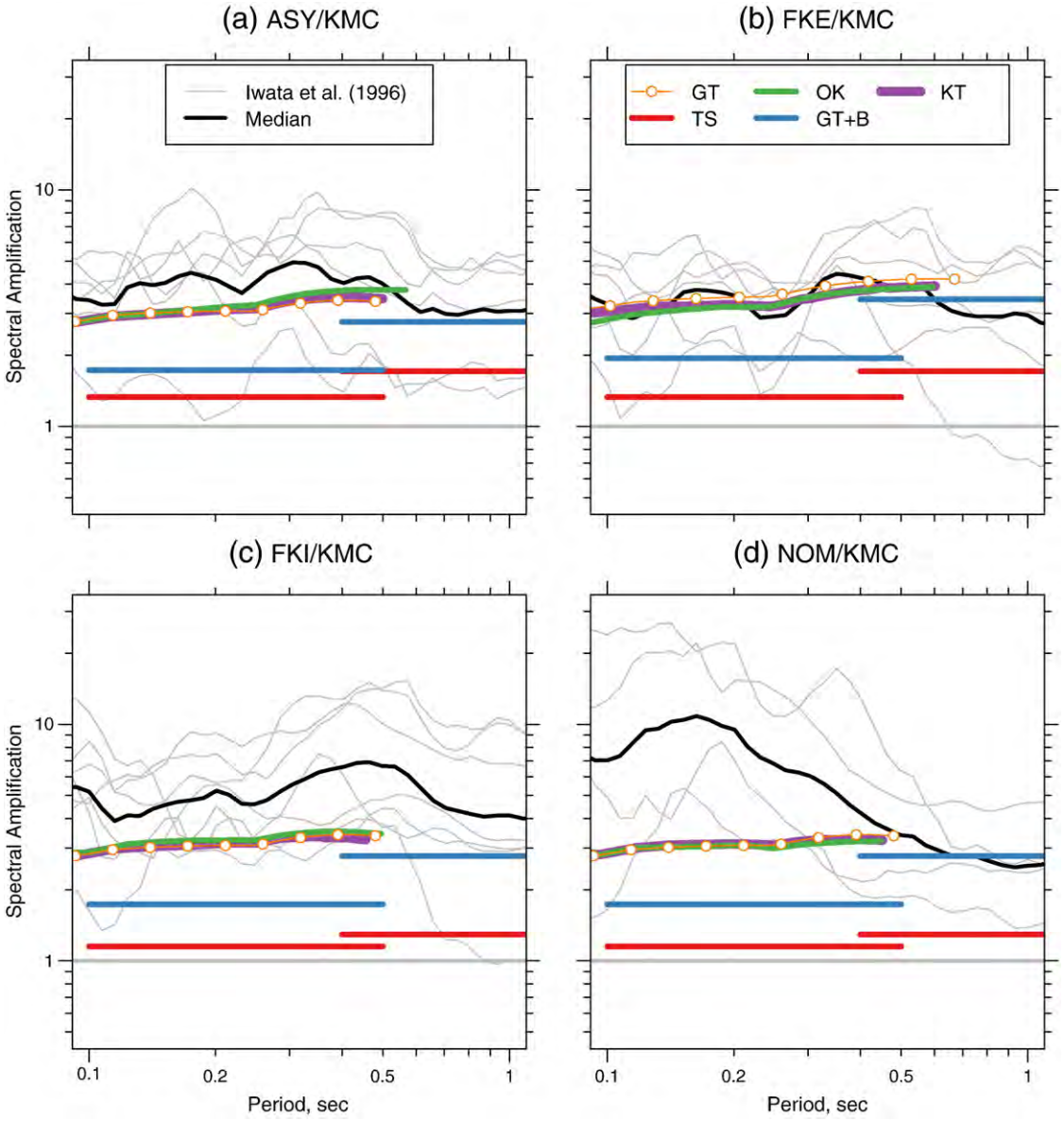

Fig. 8. Predicted response spectra amplifications for the topographic slope (TS), the geologic trend (GT), ordinary kriging (OK), kriging with a trend (KT), and the GT model combined with the Borcherdt (1994) equations (GT + B). For comparison, we include observed spectral amplifications computed from the Iwata et al. (1996) ground motion records. The gray horizontal line indicates an amplification of one (i.e., no amplification).

ASY is more accurately modeled by the GT, OK, and KT methods. Alternatively, if the inaccuracy results from more complex path effects that are not modeled by the SRI method, then improving the accuracy of $S_s^p(\mathbf{x}, \mathrm{d})$ will not improve the accuracy of $A(f)$. Analysis of ground motions in the Kobe region for the 1995 Hyogo-ken Nanbu mainshock by Pitarka et al. (1998) indicate that the three-dimensional basin structure influenced the ground motions along the basin edge. Additionally, site NOM is closest to the edge of the basin, which supports the hypothesis that the misfit at NOM is largely the result of more complex wave propagation effects.

5. Discussion

As many researchers have found, the current practice of approximating site response with correlations to $S_s(30)$ based on topography or geologic units is useful when local data are not available. This paper attempts to quantify the improvement in accuracy that can be achieved for mapping $A(f)$ when a region is uniformly sampled with additional S_s measurements.

As expected, the three methods presented here that employ local SASW measurements (GT, OK, KT) yield more accurate $A(f)$ than the TS method, which relies on global correlations (see Fig. 8). Further, the geostatistical methods (OK and KT) provide more accurate predictions of $S_s(\mathbf{x},30)$ than the GT method, which assumes homogeneous geologic units (see Fig. 6). These methods, however, require local data collection. Therefore, we propose that this method is appropriate for urban regions with moderate to high seismic risk. The cost of the local data collection can be minimized by using noninvasive in situ measurements like SASW or MASW.

Fig. 6 shows that the OK and KT models outperform the GT model in a leave-one-out cross validation of $S_s(\mathbf{x},30)$. These three methods, however, perform equally well in terms of $A(f)$. We prefer the KT model over the OK model for two reasons: First, $E = 0.40$ for the GT model, which indicates that $\mu_s(\mathbf{x},30)$ is relatively well modeled by the surficial geology; this information is incorporated in the KT model, whereas it is ignored in the OK model. Second, as distance between the location of the prediction and the observations increases, $S_s^p(\mathbf{x}, \mathrm{d})$ will approach $S_s^{\mathrm{med}}(\mathbf{x}, \mathrm{d})$ for the KT model, but $S_s^p(\mathbf{x}, d)$ will approach

$\bar{S}_s(\mathbf{x}, d)$ for the OK model. Thus, the KT model can be more seamlessly combined with a larger regional geology model, such as the Wills and Clahan (2006) model for California.

The GT, OK, and KT models predict similar amplifications at all four sites where ground motions are available to compute $a(T)$. The amplifications predicted by these methods at 3 Hz in Fig. 7 differ by as much as 25%, where the percentage difference is defined as the absolute difference divided by the arithmetic mean. These differences, however, are small relative to the differences observed in the recorded amplifications; Fig. 8 shows that the empirical amplifications vary by as much as 133% at ASY, 97% at FKE, 132% at FKI, and 146% at NOM (for $f = 3$ Hz). This underscores the limited sensitivity of one-dimensional site response models to reasonable variations of the seismic properties. Similarly, Boore and Thompson (2007) found that the theoretical site response amplifications do not vary significantly (below 5 Hz) as a 0.25 m resolution suspension log profile is approximated by coarser layers up to 10 m thick. Additionally, Thompson et al. (2009) found that the differences between the theoretical site response amplifications computed from downhole logging profiles versus SASW profiles are relatively minor even when substantial differences are observed between the two independent profiles. In contrast, if the calculation is performed in three-dimensions then reasonable variations in the seismic properties can substantially change the site response amplifications (Thompson et al., 2009).

6. Conclusions

We quantitatively demonstrate the benefit of local seismic measurements for estimating the site response spectral amplifications in an urban area. We show that geostatistical methods achieve more accurate predictions of $V_s(30)$ at unsampled locations than correlations with surficial geology or topographic slope. The differences between the OK and KT methods, in terms of the slowness estimates and the resulting amplifications, are negligible. However, we prefer the KT method because it is more easily integrated with maps of surficial geology that can cover larger regions (e.g., Wills and Clahan, 2006). Due to the increased costs of the data collection relative to the Wald and Allen (2007) topographic slope method and the Wills and Clahan (2006) geology method, the methods that we propose are appropriate for urban regions with moderate to high seismic risk. The resulting maps can be used by engineers to estimate spectral amplifications at periods of interest and the maximum usable period is controlled by the maximum depth of exploration of the seismic surveys. Spectral amplifications computed by combining a spatial model derived from local $S_s(d)$ measurements with the square root of impedance method produces more accurate estimates of observed median short-period amplifications than the topographic slope method.

Acknowledgments

The first two authors are funded by National Science Foundation Grant CMS-0547190 and the international travel and collaboration that made this work possible was funded by an International Research and Education in Engineering (IREE) supplement to CMS-0409311. We thank Tomotaka Iwata for kindly sharing the Higashinada Ward aftershock data with us. We thank Thomas Oommen and Eugene Morgan for patiently helping with GIS software. Reviews by Barbara Luke, Robb Moss, Eugene Morgan, and an anonymous reviewer substantially improved this manuscript.

References

Abercrombie, R.E., 1997. Near-surface attenuation and site effects from comparison of surface and deep borehole recordings. Bull. Seismol. Soc. Am. 87 (3), 731–744.

Asten, M.W., Boore, D.M., 2005. Comparison of shear-velocity profiles of unconsolidated sediments near the Coyote borehole (CCOC) measured with fourteen invasive and non-invasive methods. U.S. Geological Survey Open-File Report 2005-1169. 40 pp.

Baise, L.G., Lenz, J.A., Thompson, E.M., 2008. Discussion of "mapping liquefaction potential considering spatial correlations of CPT measurements" by Chia-Nan Liu and Chien-Hsun Chen. J. Geotech. Geoenviron. Eng. 134 (2), 262–263.

Boore, D.M., 2004. Can site response be predicted? J. Earthquake Eng. 8 (Special Issue 1), 1–41.

Boore, D.M., 2008. TSPP — a collection of FORTRAN programs for processing and manipulating time series. U.S. Geol. Surv. Open-File Rept. 1111.

Boore, D.M., Asten, M.W., 2008. Comparisons of shear-wave slowness in the Santa Clara Valley, California, from blind interpretations of data from a comprehensive set of invasive and non-invasive methods using active- and passive-sources. Bull. Seismol. Soc. Am. 98, 1982–2003.

Boore, D.M., Joyner, W.B., 1997. Site amplifications for generic rock sites. Bull. Seismol. Soc. Am. 87 (2), 327–341.

Boore, D.M., Thompson, E.M., 2007. On using surface-source downhole-receiver logging to determine seismic slownesses. Soil Dyn. Earthquake Eng. 27 (11), 971–985.

Boore, D.M., Watson-Lamprey, J., Abrahamson, N.A., 2006. Orientation-independent measures of ground motion. Bull. Seismol. Soc. Am. 94 (4A), 1502–1511.

Borcherdt, R.D., 1970. Effects of local geology on ground motion near San Francisco Bay. Bull. Seismol. Soc. Am. 60 (1), 29–61.

Borcherdt, R.D., 1994. Estimates of site-dependent response spectra for design (methodology and justification). Earthquake Spectra 10, 617–654.

Brown, L.T., Boore, D.M., Stokoe, K.H., 2002. Comparison of shear-wave slowness profiles at 10 strong-motion sites from noninvasive SASW measurements and measurements made in boreholes. Bull. Seismol. Soc. Am. 52, 289–300.

Cambardella, C.A., Moorman, T.B., Novak, J.M., Parkin, T.B., Karlen, D.L., Turco, R.F., Konopka, A.E., 1994. Field-scale variability of soil properties in central Iowa soils. Soil Sci. Soc. Am. J. 58 (5), 1501–1511.

Cressie, N.A.C., 1993. Statistics for Spatial Data. John Wiley & Sons, Inc., New York.

Diggle, P.J., Ribeiro, P.J., 2006. Model-based Geostatistics. Springer, New York.

Farr, T.G., Kobrick, M., 2000. Shuttle radar topography mission produces a wealth of data. EOS 81, 583â€"585.

Goovaerts, P., 1999. Geostatistics in soil science: state-of-the-art and perspectives. Geoderma 89, 1–45.

Guttorp, P., Gneiting, T., 2005. On the Whittle-Matérn correlation family. Tech. Rep. 81, University of Washington, NRCSE Technical Report Series. .

Harrell Jr., F.E., 2006. Regression Modeling Strategies. Springer-Verlag New York, Inc.

Haskell, N.A., 1953. The dispersion of surface waves on multilayered media. Bull. Seismol. Soc. Am. 72, 17–34.

Holzer, T.L., Padovani, A.C., Bennett, M.J., Noce, T.E., Tinsley, J.C., 2005. Mapping NEHRP Vs30 site classes. Earthquake Spectra 21 (2), 353–370.

ICC, 2006. International Building Code (IBC). International Code Council (ICC), Falls Church, Virginia.

Iwata, T., Hatayama, K., Kawase, H., Irikura, K., 1996. Site amplification of ground motions during aftershocks of the 1995 Hyogo-ken Nanbu earthquake in severely damaged zone — array observation of ground motions in Higashinada ward, Kobe City, Japan. J. Phys. Earth 44 (5), 553–561.

Joyner, W.B., Warrick, R.E., Fumal, T.E., 1981. The effect of quaternary alluvium on strong ground motion in the Coyote Lake, California, Earthquake of 1979. Bull. Seismol. Soc. Am. 71 (4), 1333–1349.

Kayen, R.E., Thompson, E.M., Minasian, D., Carkin, B., 2005. Shear-wave velocity of the ground near sixty California strong motion recording sites by the spectral analysis of surface waves (SASW) method and harmonic-wave sources. U.S. Geological Survey Open-File Report 2005–1366, 132 pp. available from http://pubs.usgs.gov/of/2005/1366.

Kayen, R., Moss, R. E. S., Thompson, E. M., Seed, R. B., Cetin, K. O., Der Kiureghian, A., Tanaka, Y., Tokimatsu, K., 2010. Probabilistic and deterministic assessment of seismic soil liquefaction potential by shear wave velocity, submitted to *J. Geotech. Geoenv. Eng.*

Kramer, S.L., 1996. Geotechnical Earthquake Engineering. Prentice Hall.

Lay, T., Wallace, T.C., 1995. Modern Global Seismology. Academic Press, San Diego.

Legates, D.R., McCabe, G.J., 1999. Evaluating the use of "goodness-of-fit" measures in hydrologic and hydroclimatic model validation. Water Resour. Res. 35 (1), 233–241.

Morgan, E.C., McAdoo, B.G., Baise, L.G., 2008. Quantifying geomorphology associated with large subduction zone earthquakes. Basin Res. 20 (4), 531–542.

Nazarian, S., Stokoe, K.H., 1984. In-situ shear wave velocities from spectral analysis of surface waves. : Proceedings of the Eighth World Conference on Earthquake Engineering, vol. III. Prentice-Hall, Englewood Cliffs, New Jersey, pp. 31–38.

Park, C., Miller, R., Xia, J., 1999. Multichannel analysis of surface waves. Geophysics 64 (3), 800–808.

Pitarka, A., Irikura, K., Iwata, T., Sekiguchi, H., 1998. Three-dimensional simulation of the near-fault ground motion for the 1995 Hyogo-ken Nanbu (Kobe), Japan, earthquake. Bull. Seismol. Soc. Am. 88 (2), 428–440.

R Development Core Team, 2009. R: A Language and Environment for Statistical Computing. R Foundation for Statistical Computing, Vienna, Austria3-900051-07-0. URL http://www.R-project.org.

Shearer, P.M., 1999. Introduction to Seismology. Cambridge University Press.

Shearer, P.M., Orcutt, J.A., 1987. Surface and near-surface effects on seismic-waves—theory and borehole seismometer results. Bull. Seismol. Soc. Am. 77 (4), 1168–1196.

Stokoe, K.H., Rix, G.L., Nazarian, S., 1989. In-situ seismic testing with surface waves: Proceedings of the Twelfth International Conference on Soil Mechanics and Foundation Engineering, vol. 1, pp. 330–334. rio de Janeiro, Brazil.

Thompson, E.M., Baise, L.G., Kayen, R.E., 2007. Spatial correlation of shear-wave velocity in the San Francisco Bay Area sediments. Soil Dyn. Earthquake Eng. 27 (2), 144–152.
Thompson, E.M., Baise, L.G., Kayen, R.E., Guzina, B.B., 2009. Impediments to predicting site response: seismic property estimation and modeling simplifications. Bull. Seismol. Soc. Am. 99 (5), 2927–2949.
Thomson, W.T., 1950. Transmission of elastic waves through a stratified solid. J. Appl. Phys. 21, 89–93.
Tinsley, J.C., Fumal, T.E., 1985. In: Ziony, J.I. (Ed.), Mapping quaternary sedimentary deposits for areal variations in shaking response: Evaluating Earthquake Hazards in the Los Angeles Region-An Earth Science Perspective, pp. 101–125.
Wald, D.J., Allen, T.I., 2007. Topographic slope as a proxy for seismic site conditions and amplification. Bull. Seismol. Soc. Am. 97 (5), 1379–1395.
Wessel, P., Smith, W.H.F., 1991. Generic mapping tools. EOS 72, 441.
Wills, C.J., Clahan, K.B., 2006. Developing a map of geologically defined site-condition categories for California. Bull. Seismol. Soc. Am. 96 (4), 1483–1501.
Wills, C.J., Silva, W., 1998. Shear-wave velocity characteristics of geologic units in California. Earthquake Spectra 14 (3), 533–556.
Wills, C.J., Petersen, M., Bryant, W.A., Reichle, M., Saucedo, G.J., Tan, S., Taylor, G., Treiman, J., 2000. A site-conditions map for California based on geology and shear-wave velocity. Bull. Seismol. Soc. Am. 90 (6 PT B), 187–208.
Yong, A., Hough, S.E., Abrams, M.J., Cox, H.M., Wills, C.J., Simila, G.W., 2008. Site characterization using integrated imaging analysis methods on satellite data of the Islamabad, Pakistan, Region. Bull. Seismol. Soc. Am. 98 (6), 2679–2693.